



RESEARCH PAPER

Digital Twins for Post-Earthquake Loss Assessment of Building Portfolios

Amir Taherian¹ | Vitor Silva^{1,2} | Al Mouayed Bellah Nafeh² | Gerard J. O'Reilly³

¹CERIS, Department of Civil Engineering, University of Aveiro, Aveiro, Portugal | ²Global Earthquake Model (GEM) Foundation, Pavia, Italy | ³Istituto Universitario di Studi Superiori (IUSS), Pavia, Italy

Correspondence: Amir Taherian (ar.taherian@ua.pt)

Received: 29 September 2025 | **Revised:** 4 May 2026 | **Accepted:** 1 June 2026

ABSTRACT

Conventional earthquake impact assessments often rely on broad assumptions and simplified models, which introduce significant uncertainty into building damage predictions. Although recent advances in machine learning, detailed building inventories, and low-cost sensors have created opportunities for more refined analyses, these tools have not yet been comprehensively evaluated at the portfolio scale. To address this gap, this study presents a digital twin framework validated through comprehensive virtual experiments. The proposed system is designed to integrate ML-based damage data with real-time sensor data, thereby reducing the bias and uncertainty inherent in traditional methods. The approach is demonstrated through the development of a detailed digital twin of the Alvalade parish in Lisbon, Portugal, where advanced simulations were used to evaluate building responses under earthquake scenarios. Sensor placement strategies were also examined to further minimize uncertainty. Results from this computational validation demonstrate the theoretical potential for digital twins to substantially improve damage assessment accuracy, providing a framework for future real-world implementation and operational deployment.

1 | Introduction

The increasing number of people and assets in urban areas worldwide, together with the growing severity and impact of natural hazards, underscores a vital and increasing need for advanced and precise methods to evaluate and manage urban seismic risk. As of 2025, approximately 56% of the global population resides in urban areas, a figure projected to rise to 68% by 2050, adding around 2.5 billion people to urban centers, predominantly in Asia and Africa (He et al. 2021). This rapid urban growth often results in the spread of informal settlements and the construction of buildings that may not meet seismic safety standards, which increases their vulnerability to earthquakes (Giordano et al. 2023; Ozsarac et al. 2025).

Conventional seismic risk assessment methods largely rely on regional ground motion data and generalized building vulnerability models. While these approaches provide essential inputs for risk management, the broad assumptions required for generalized application introduce significant uncertainty, sometimes resulting in biased risk estimates (Erdik 2017; Zhao et al. 2023). However, recent advances signal a paradigm shift from reactive to proactive disaster management through the use of *digital twins*. A *digital twin* is a high-fidelity virtual replica of a physical system that remains continuously synchronized with its real-world counterpart via real-time data streams (Mohammadi and Taylor 2017, 2021). Unlike static models, *digital twins* enable dynamic simulations, predictive analytics, and informed

decision-making, offering an evolving representation of complex systems. These capabilities are increasingly powered by machine learning (ML) and the widespread availability of low-cost sensors, making it possible to predict and monitor the seismic response of individual buildings with unprecedented precision (Li and Brennan 2024). To date, *digital twins* applications have been most successful at the scale of single structures, particularly for critical infrastructure like bridges (Ye et al. 2019). However, a major gap remains: the absence of scalable frameworks that integrate real-time sensor data and ML-based predictions to support portfolio-level seismic risk assessment and rapid earthquake impact evaluation. Bridging this gap is essential for advancing city-scale seismic vulnerability analysis and enabling more effective disaster response and long-term resilience planning.

To address this research gap, this study proposes an urban area *digital twin* for rapid earthquake impact assessment. This research is guided by three primary objectives: (1) to develop a robust digital twin framework capable of simulating detailed, building-specific seismic responses via comprehensive benchmark analyses applied to a real urban context, specifically the Alvalade district of Lisbon; (2) to evaluate the influence of alternative sensor deployment strategies and data integration methodologies on the accuracy and potential bias in earthquake impact estimates; and (3) to quantify the extent to which real-time sensor data usage can reduce uncertainty in portfolio-level seismic risk assessment relative to conventional approaches. Through these objectives, this study contributes to advancing *digital twin* methodologies and provides valuable insights for their application to support portfolio risk analysis.

2 | Review of Past Studies on Digital Twins

Smart City Digital Twins (SCDTs) represent a transformative tool for disaster management, linking physical and digital environments through real-time data exchange. The UK's National Digital Twin Program defines them as “realistic digital representations of assets, processes, and systems” with continuous data connectivity (Bolton et al. 2018). Lu et al. (2020) describe *digital twins* as “living digital simulation models that are able to learn and update from multiple sources,” while Mikell and Mikell (2018) highlight their life-cycle adaptability for decision-making through real-time calibration. The foundational model by Grieves (2002) identifies three essential elements: physical entities, virtual entities, and bidirectional communication links. This synchronization, governed by the “twinning rate” (Pregolato et al. 2022), has been further enhanced by Brucherseifer et al. (2025), who proposed a disaster-specific data taxonomy and similarity function, addressing data scarcity during emergencies through alternative data source identification. Other interesting frameworks for the development of *digital twins* have been proposed by Lu et al. (2020) and Yu et al. (2023).

One of the first implementations of a real *digital twin* is the Flood Alert System (FAS) at Houston's Texas Medical Center. This system accurately predicted peak flow and timing during a 2015 flood, with a 0.83% margin of error and a 35 min deviation, offering 2–3 h of lead time for flood defenses (Ford and Wolf 2020).

In the seismic domain, applications range from UAV-based postearthquake damage imagery (Hoskere et al. 2022), high-fidelity simulations (Kusakabe et al. 2021), bridge collapse risk estimation (Lin et al. 2021), and postearthquake structural tagging (Levine and Spencer 2022), to automated finite element modeling using imagery (Pantoja-Rosero et al. 2023). Emerging systems like those proposed by Habib et al. (2025) and Yu et al. (2023) combine real-time monitoring with urban resilience frameworks. Dal Zilio et al. (2023) present a future vision where earthquake *digital twins* provide after-shock forecasting, rapid ground shaking maps, and fault rupture modeling, potentially offering time-critical updates for early warning systems. Yet, despite such progress, comprehensive city-scale seismic *digital twins* remain conceptual. Major gaps persist in city-scale seismic digital twins, including portfolio-level structural response prediction with real-time sensor integration, infrastructure network interdependencies, population mobility dynamics, and emergency service coordination. While comprehensive urban resilience assessment requires addressing all these components, this study specifically focuses on the first gap: developing a sensor-informed framework for building portfolio response prediction.

Parallel advances in artificial intelligence (AI), AI of things (AIoT) and edge computing have accelerated SCDT capabilities (Dogan et al. 2021; Li 2022). For example, AIoT-enabled fire systems can forecast ignitions within 60 s when coupled with spatiotemporal temperature models (Xie et al. 2025). These technologies collectively transition static models into dynamic, evolving systems (Lu et al. 2020; Mohammadi and Taylor 2017), capable of operating on multiple temporal scales: from rapid earthquakes to slow climate events, tackling what Mohammadi and Taylor (2017) describe as the “thinking fast and slow” challenge (Ford and Wolf 2020).

While literature demonstrates significant advances in *digital twins* for disaster management, this study narrows its focus to a critical yet underexplored component: real-time structural response prediction for building portfolios during seismic

events. From the review of these existing studies, we propose a structured, multilayered digital twin framework tailored specifically for seismic impact assessment at the building portfolio scale, as illustrated in Figure 1. The framework comprises:

1. Physical layer: Detailed characterization of exposed assets, including building attributes such as structural typology, height, primary construction material, and construction period;
2. Sensor layer: Deployment of real-time monitoring equipment (e.g., accelerometers) between and within representative structures.
3. Data processing layer: ML and surrogate models coupling real-time sensor data with nonlinear time-history analyses (NLTHA) to predict building-level damage states (DSs).
4. Digital twin layer: Continuous updating of virtual entities to reflect the actual structural condition detected across the investigated portfolio of exposed assets.
5. Decision support layer: Production of actionable outputs or real-time impact estimation, prioritization of inspections, and emergency planning.

By integrating the *digital twin* across all five layers, this framework provides a scalable (i.e., computationally efficient for large building portfolios and extensible from neighborhood to regional scales) and operational pathway for dynamic seismic risk management at the urban scale.

3 | Methodology

The proposed digital twin framework leverages the principle that seismic responses from a strategically instrumented subset of buildings can be extrapolated to improve predictions for the entire portfolio, avoiding the impracticality of full-scale sensor deployment. The approach assumes that buildings with similar structural characteristics exhibit comparable seismic behavior. However, the validation of the proposed framework is challenged by the scarcity of real earthquake data, which rarely captures diverse ground motions with sufficient instrumentation to assess building-specific responses at scale. To address this, large synthetic datasets of ground motion records and structural response histories are generated using stochastic simulations and NLTHA, respectively. Subsequently, the datasets are divided into two subsets: a training

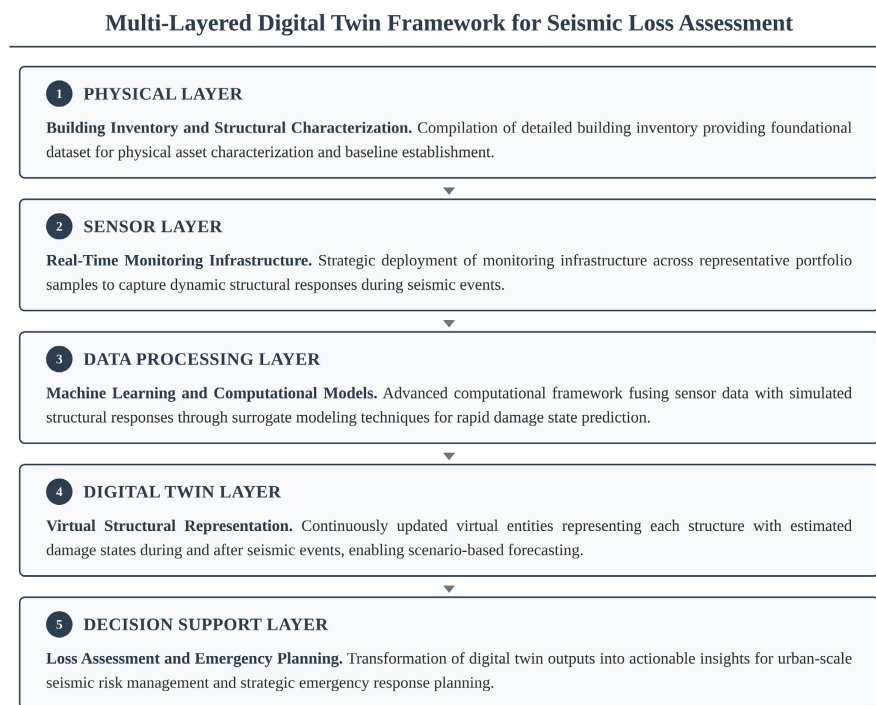


FIGURE 1 | Multilayered digital twin framework for portfolio-scale seismic loss assessment, integrating building inventory, sensor data, computational models, virtual representations, and decision-support tools for real-time earthquake risk management.

set for the development of an ML model to predict the structural response of the building portfolio following earthquake ground shaking, and a testing set to evaluate the predictive performance of the ML model. The methodology, summarized in Figure 2, consists of seven steps:

- Step 1 – Structural Capacity Definition: Each building in the investigated portfolio is assigned a capacity model (i.e., force–deformation relationship) using the vulnerability model from Martins and Silva (2021) and based on key structural characteristics following the GEM Taxonomy (Silva et al. 2022);
- Step 2 – Generation of Synthetic Ground Motion Records: A large dataset of seismic events is simulated using the hazard model for Portugal, and for each event, several synthetic ground motion records are generated using stochastic simulations; the dataset is then split into Subset 1 and Subset 2;
- Step 3 – Development of the ML Model: NLTHA is performed using Subset 1 on all modeled buildings of the investigated portfolio. These NLTHA results are then used to calibrate an ML model to predict building response based on a set of intensity measures (IMs).
- Step 4 – Benchmark Results Production (Method A): The structural response and portfolio losses are evaluated based on NLTHA results using Subset 2 of synthetic records. These results represent the “ground truth”.
- Step 5 – Loss Estimation with ML Model Only (Method B): Portfolio losses for each event in Subset 2 are evaluated via the trained ML model, without considering sensor data.
- Step 6 – Loss Estimation Using the *Digital Twin* (Method C): Portfolio losses for each event in Subset 2 are evaluated by combining ML model predictions with data from hypothetical sensors located on a set of representative building classes. Additionally, the optimal number of sensors per building class is investigated.

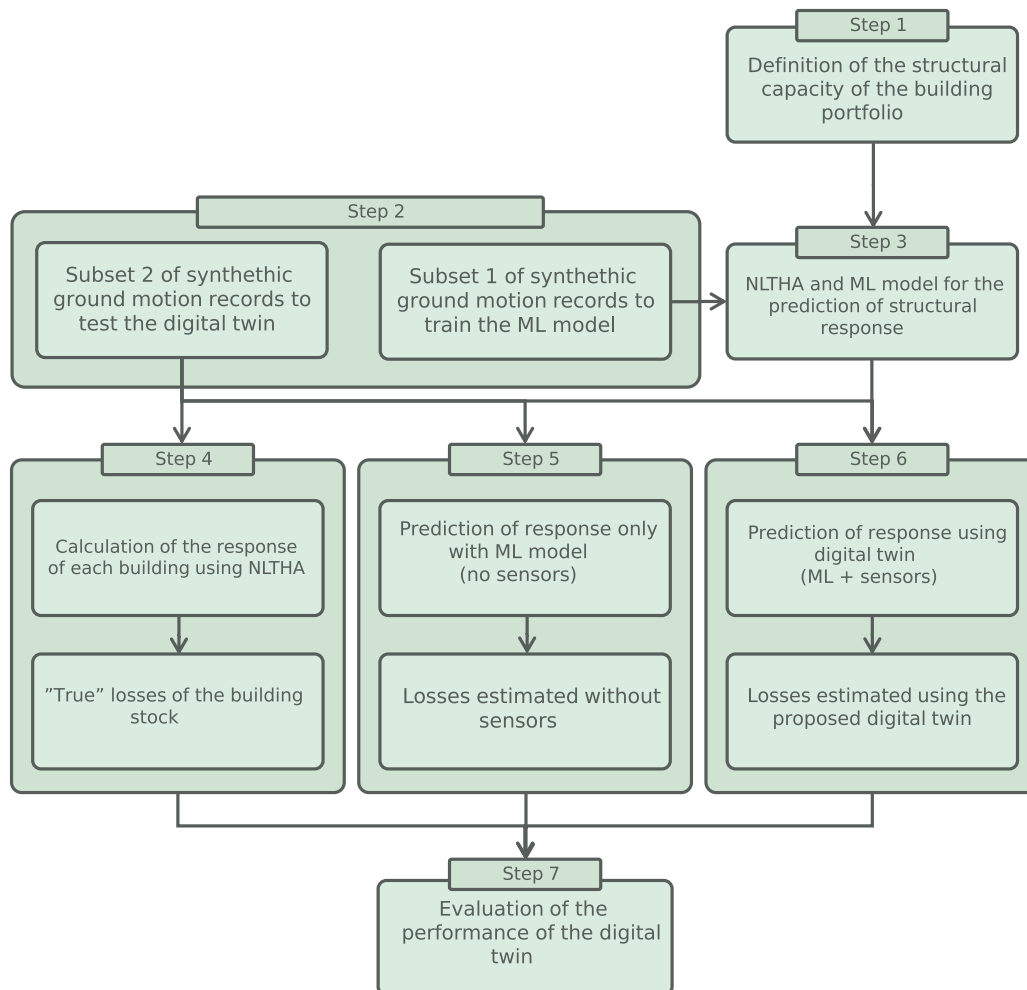


FIGURE 2 | Flowchart illustrating the methodology for the development and testing of the *digital twin*.

- Step 7 – *Digital Twin* Performance Evaluation: Portfolio losses from Methods B (ML only) and C (*digital twin*) are compared against Method A (benchmark) to quantify improvements in prediction accuracy and reduction of bias and uncertainty.

Each step is described in detail in the following subsections.

3.1 | Step 1 – Capacity Definition for the Building Portfolio

The Alvalade parish building inventory, comprising 2457 structures, was sourced from Silva et al. (2024) and classified according to the GEM Taxonomy (Silva et al. 2022) into 66 unique building classes (see Figure 3). Reinforced concrete (CR) buildings (1187) are mainly concentrated in the central and eastern areas in organized grid patterns, while unreinforced masonry (MUR) buildings (1265) are dispersed across the district with clusters in the western and northern sections reflecting earlier construction periods. As shown in Figure 4, only two MUR classes (MUR/LWAL + CDL/H2 and MUR/LWAL + CDL/H4) encompass over 1200 structures, highlighting substantial structural clustering that may produce correlated seismic response patterns during earthquake events, making this inventory particularly valuable for testing *digital twin* frameworks.

To create a realistic case study for the *digital twin*, the structural capacity of Alvalade’s building portfolio was characterized using simplified capacity models, which describe the relationship between equivalent lateral seismic force demand and displacement response for a building. These models provide essential information on how buildings yield, deform, and ultimately fail when subjected to earthquake shaking. The capacity curves of Martins and Silva (2021) were adopted as the median curve for each building class. To capture variability in geometric, material, and mechanical properties within each class, individual building capacity curves were sampled around the median, assuming a lognormal distribution for yielding and ultimate points. A standard deviation of $\beta = 0.3$ was applied to both points, consistent with previous studies (Silva et al. 2014; FEMA 2020). Figure 5 illustrates this process for the most common building class, showing the median curve alongside the sampled variations, expressed in terms of spectral acceleration and spectral displacement.

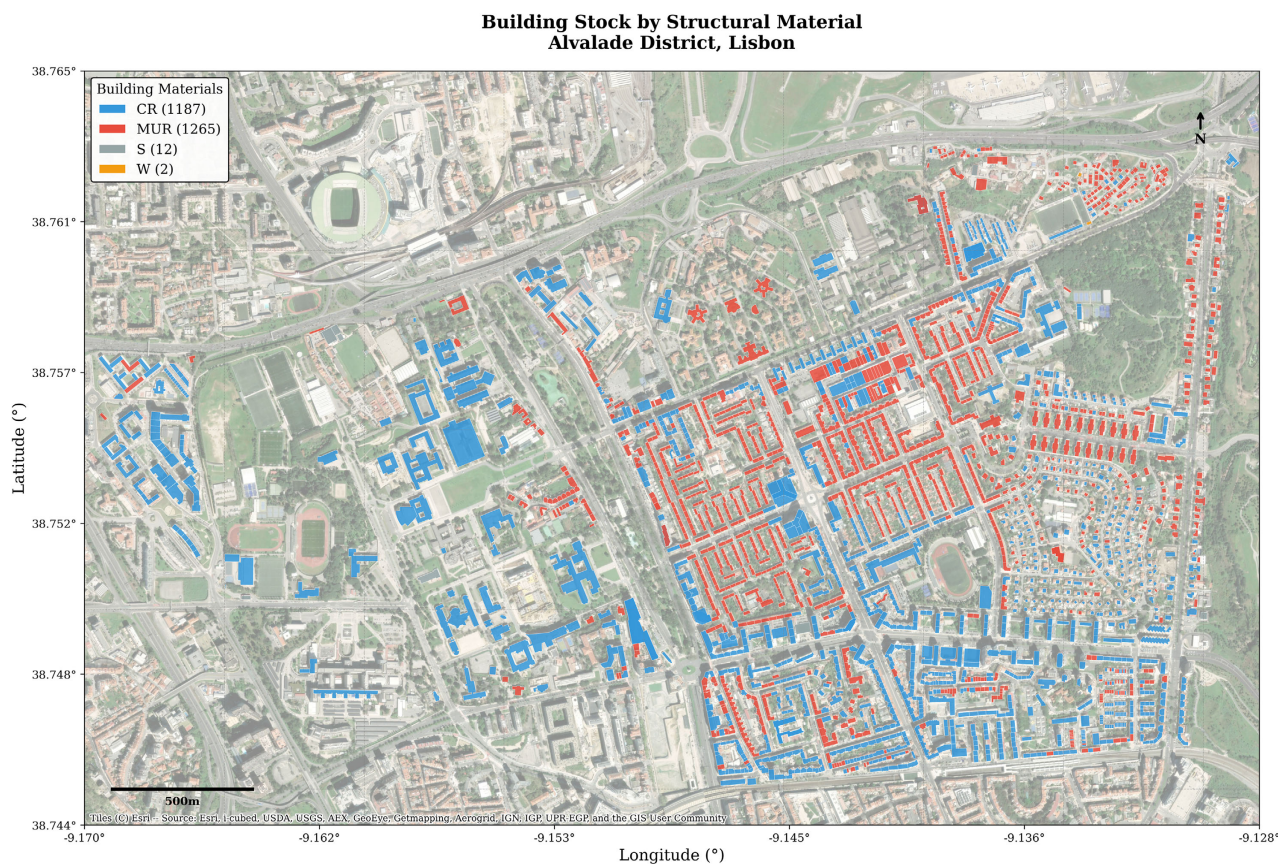


FIGURE 3 | Building stock distribution in Alvalade parish (district of Lisbon) classified according to the GEM taxonomy: CR - reinforced concrete, MUR - unreinforced masonry, S - steel, and W - wood.

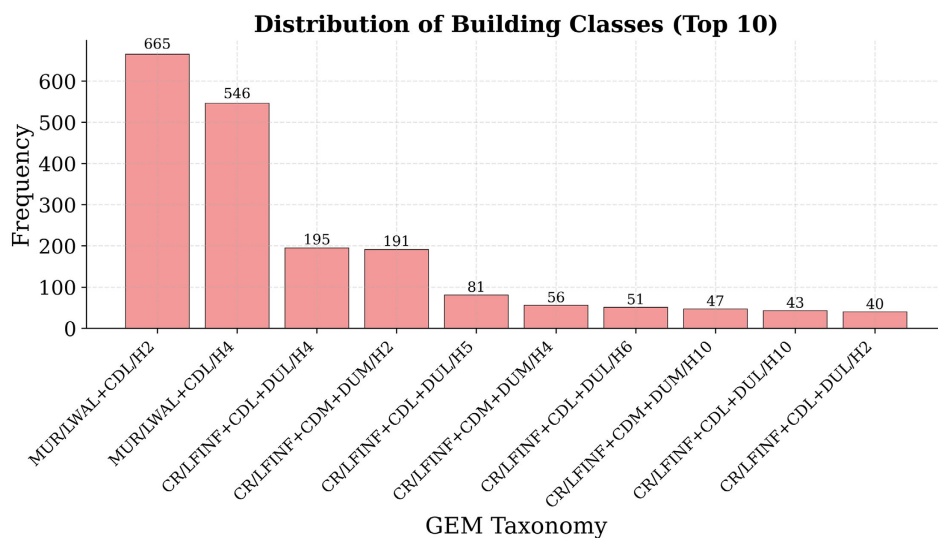


FIGURE 4 | Distribution of building classes (top 10 building classes which cover 85% of the entire portfolio) based on the GEM taxonomy classification. Building class codes represent structural material types: MUR - Unreinforced masonry, CR - Reinforced concrete; lateral load-resisting systems: LWAL - Wall, LFINF - Infilled frame; code levels: CDL - low code, CDM - moderate code; ductility levels: DUL - low ductility; and height categories: H followed by number indicates building stories (e.g., H2 - 2 stories).

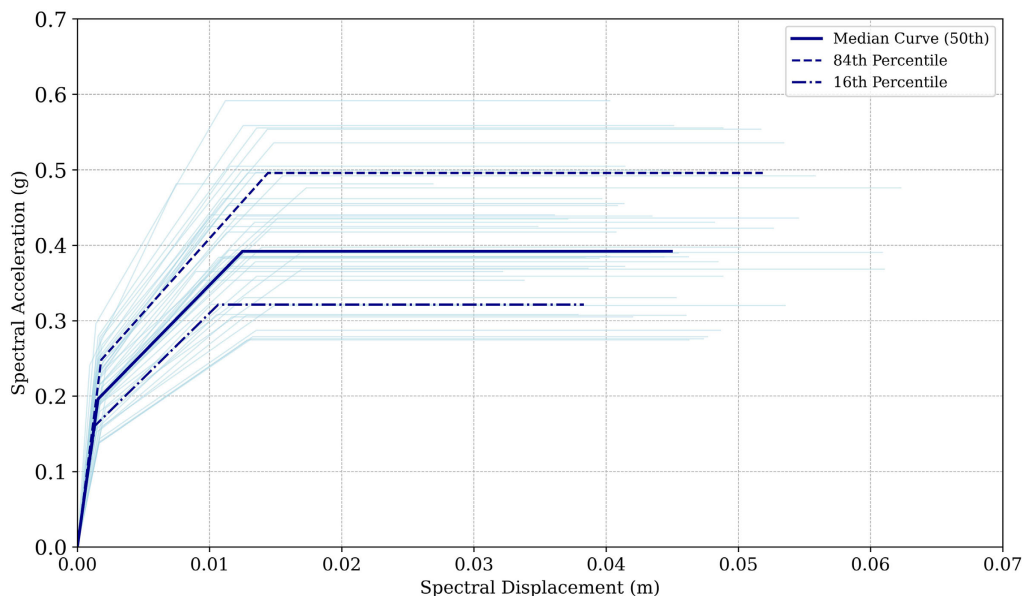


FIGURE 5 | Generated capacity curves for MUR/LWAL + CDL/H2 building type showing the 16th percentile, median, and 84th percentile responses in acceleration-displacement space.

Using the sampled capacity curves, each building was represented as an idealized “stick-and-mass” multidegree-of-freedom (MDOF) system (Khaloo and Khosravi 2013), where the global capacity curves serve as calibration targets for distributing story-level force–displacement relationships through mode shape analysis. Each floor is modeled as a lumped mass connected with zero-length elements coupled with *Pinching4* hysteretic material models to capture story-based strength and stiffness degradation under cyclic loading. Fundamental mode shapes were obtained via *eigenvalue* analysis, accounting for different building typologies and potential soft-story irregularities. Rayleigh damping was applied using the first and third modes with a 5% damping ratio, and Newmark integration with adaptive time-stepping was used to ensure numerical convergence. This process produces a virtual representation of the Alvalade parish, enabling millions of NLTHA using synthetic ground motion records generated for the region as illustrated in Figure 6.

While the stick-and-mass modeling framework was originally developed for moment-resisting frames (Khaloo and Khosravi 2013), the capacity curves themselves are derived from Martins and Silva (2021), which provide class-specific

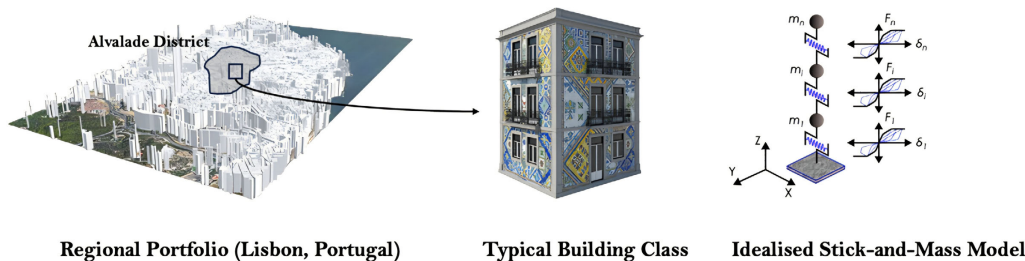


FIGURE 6 | Numerical representation of the Alvalade civil parish in Lisbon via idealized stick-and-mass MDOF systems used for city-scale NLTHA.

curves defined based on experimental data, observed damage, numerical analysis, and expert judgment for diverse typologies including URM structures. These curves inherently capture the aggregate effects of URM-specific behavior (lower ductility, reduced postyield stiffness) through their characteristic shape, though detailed failure mechanisms (diagonal cracking, in-plane/out-of-plane interaction, rocking) are not explicitly modeled at the element level. This simplification is consistent with portfolio-scale vulnerability assessment practice, where detailed micromodeling is computationally prohibitive for large building populations.

3.2 | Step 2 – Generation of Synthetic Ground Motion Records

A large stochastic event set comprising 14,000 rupture scenarios for the Western Iberian Peninsula was generated using the European seismic hazard model (Danciu et al. 2021). This catalog was subsequently filtered to retain only magnitude-distance combinations producing peak ground acceleration (PGA) exceeding 0.05 g, ensuring computational efficiency while preserving all scenarios with significant damage potential. After filtering, 2000 rupture scenarios were selected for detailed analysis. The resulting catalog provides comprehensive coverage of the magnitude-distance space relevant for seismic risk assessment in the region, as illustrated in Figure 7. The distance distribution over magnitude bins captures both near-field scenarios from moderate inland earthquakes (M6.0-7.5) and far-field scenarios dominated by larger offshore events (M7.5-9.0) capable of generating long-period ground motions despite greater source distances. While the stated ranges represent the bulk of filtered events (1st–99th percentile), the catalog includes a small number of lower and higher magnitude events that produce significant ground motion ($PGA > 0.05$ g) in the study area.

Stress drop parameters were calibrated for the Western Iberian Peninsula following Taherian et al. (2024). The resulting frequency distribution confirms the physical realism of the rupture scenarios; inland events exhibit stress drops concentrated around 50bars, whereas offshore events display higher stress drops centered on 140 bars with broader variability, reflecting the complex tectonic environments and deeper seismogenic zones characteristic of oceanic transform boundaries.

For each rupture scenario, acceleration time histories were generated using a stochastic finite-fault methodology (Boore 2003). Site amplification effects were incorporated using a representative V_{S30} value of 300 m/s, derived from the median of three available site measurements in Alvalade (ranging from 272.5 to 351.5 m/s). The amplification model of Stewart et al. (2020), originally developed for Central and Eastern North America, was adopted due to the comparable seismotectonic setting. Both Lisbon and CENA regions are characterized by stable continental interiors with high-impedance bedrock ($V_{S30} > 800$ m/s in many locations) overlain by softer sedimentary deposits, producing similar site amplification characteristics that make this model more appropriate than those calibrated to active tectonic regions. Further details on stochastic ground motion generation for Western Iberia are provided in Taherian et al. (2024). Synthetic accelerograms were generated at 20 locations uniformly distributed across Alvalade. These locations represent hypothetical seismic stations that could be integrated into the proposed *digital twin*, ensuring comprehensive spatial coverage of ground motion variability. Figure 8 presents the pseudo spectral acceleration (PSA) distributions across vibration periods (T) relevant to the local building classes.

The final catalog of 2000 rupture scenarios was divided into two subsets. A training subset of 1400 events (70%) was used for ML model development and calibration, while the remaining 600 events (30%) were reserved as an independent testing subset to evaluate the performance of the *digital twin*.

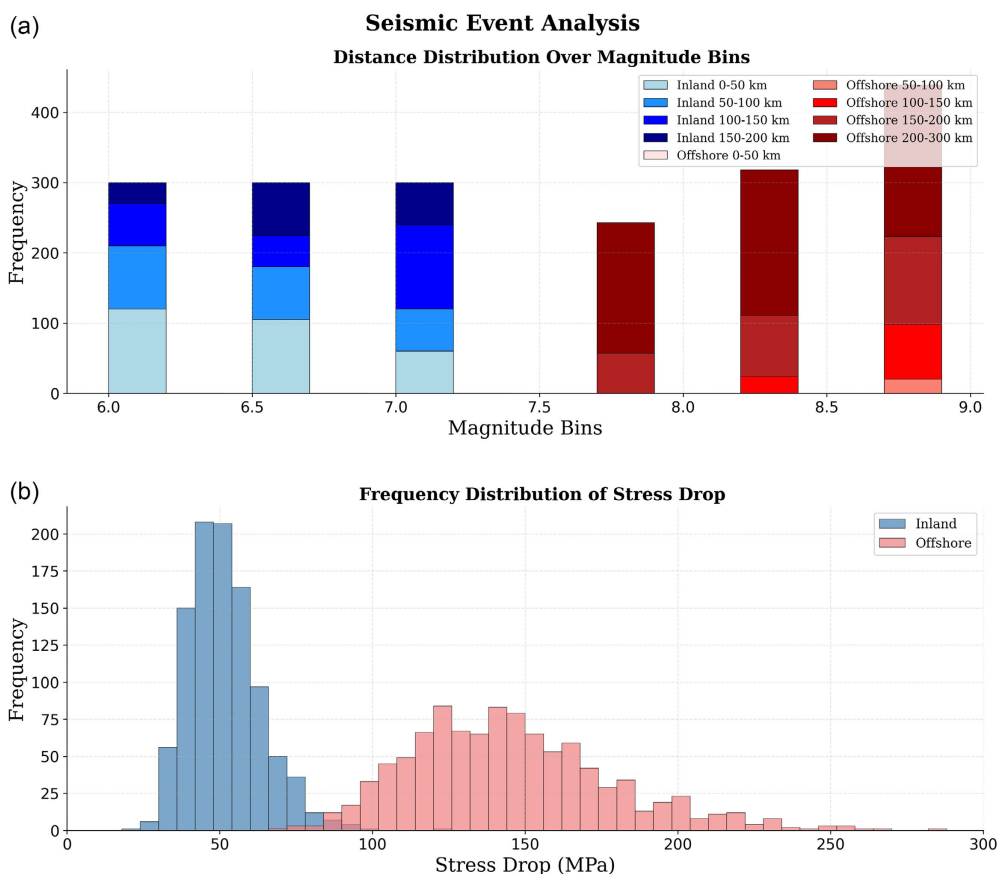


FIGURE 7 | (a) Distance distribution over magnitude bins of the filtered event set and (b) frequency distribution of stress drop showing inland events concentrated around 50 bars and offshore events around 140 bars with broader variability.

3.3 | Step 3 – ML Model for the Prediction of Structural Response

To enable rapid structural response prediction without the computational burden of repeated NLTHA, artificial neural network (ANN) models were developed to learn the complex mapping between ground motion characteristics and building response. To this end, NLTHA were performed for each building in the region using synthetic ground motion records from Subset 1 and the OpenQuake Vulnerability Modelers Toolkit¹ (Nafeh et al. 2025), resulting in nearly five million individual analyses. The maximum roof displacement was extracted from each analysis as the primary engineering demand parameter (EDP), chosen for its simplicity, compatibility with available damage-to-loss models, and measurability with low-cost sensors.

An ANN was trained to instantly predict structural response based on a set of IMs, including PGA, spectral acceleration (Sa(T)), and average spectral acceleration (AvgSA), defined as the geometric mean of spectral accelerations over the period range 0.2–1.5 s around the conditioning period $T = 0.6$ s. A feed-forward architecture with multiple hidden layers was employed, incorporating dense layers with ReLU activations, batch normalization, dropout, and L2 regularization to enhance stability, prevent overfitting, and ensure high predictive accuracy (Kalakonas and Silva 2022). The natural logarithm of maximum roof displacement was used as the target output. A fivefold cross-validation strategy (Farrar and Worden 2012) with early stopping and model checkpointing was applied to ensure robust performance, allowing the ANN to reliably predict responses for previously unseen earthquake scenarios. Model evaluation demonstrated satisfactory predictive capability across the building portfolio. For example, for the CR/LFINF + CDL + DUL/H6 building class, predicted versus “true” values showed strong linear correlation, with R^2 values of 0.901 for training and 0.897 for testing, indicating that the model successfully captures the underlying relationships between IMs and structural response (Figure 9). The model captures 99% of responses with high accuracy, with apparent saturation at extreme displacement values (>1.1 m) affecting less than 1% of the data, which are outliers from numerical instabilities rather than typical structural behavior. It is important to note that while the global R^2 values indicate strong overall performance, proportionally larger relative errors can occur in the low-displacement range where DS transitions occur, as the high R^2 is influenced by variance across the full dataset and may mask errors at these critical thresholds that primarily affect

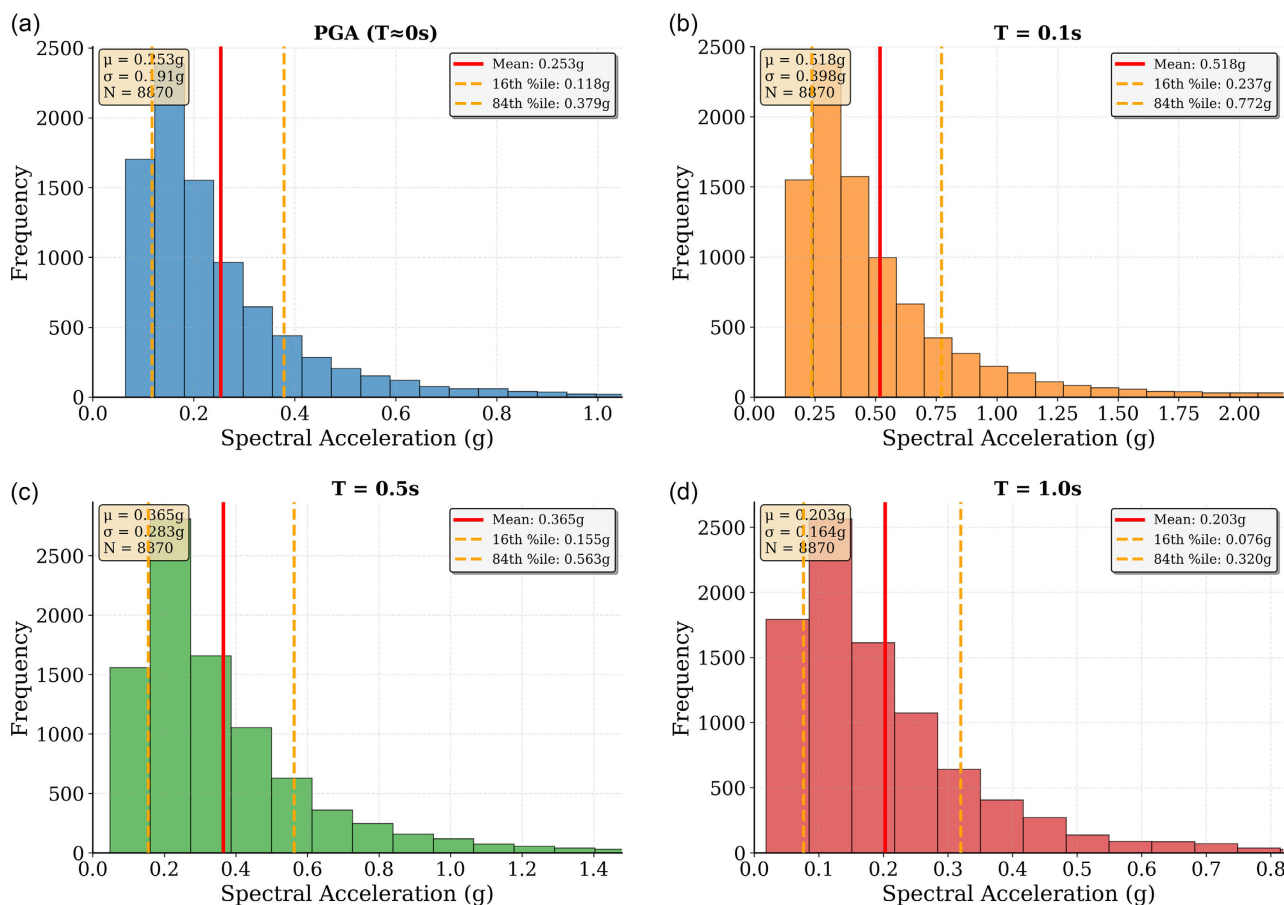


FIGURE 8 | (a) PSA Distributions of PGA and spectral acceleration for (b) $T = 0.1$ s, (c) $T = 0.5$ s, and (d) $T = 1.0$ s.

moderate-intensity events. The ANN model is available to the scientific community in a public repository: <https://github.com/amirt1994/Alvalade-seismic-digital-twin>.

3.4 | Step 4 – Generation of the Benchmark Results (Method A)

To generate the benchmark results that are used to evaluate the proposed *digital twin*, NLTHA were carried out on each building using the synthetic ground motion records from Subset 2. To this end, DS were assigned directly by comparing the maximum roof displacement obtained from the NLTHA results against the DS thresholds established by Martins and Silva (2021). Each building was categorized into one of five discrete DSs (DS0: no damage, DS1: slight, DS2: moderate, DS3: extensive, and DS4: complete) based on whether its peak roof displacement exceeds the corresponding threshold values. For each earthquake scenario, the full distribution of DSs was computed, providing the baseline structural response patterns that the *digital twin* must reproduce, as shown in Figure 10.

The spatial earthquake impact footprint for rupture scenario #950, shown in Figure 11, illustrates how small variations in ground motion intensity can produce diverse damage outcomes due to differences in building capacity. For this scenario, PGA values at the 20 synthetic station locations across the district ranged from 0.45 to 0.55 g. A total of 1515 buildings remained undamaged, primarily in areas of slightly lower shaking, while 319 buildings reached complete DS (i.e., DS4), concentrated in zones of peak intensity. Additionally, 117 buildings were classified as extensively damaged and 265 as moderately damaged. These spatial patterns reflect both the distribution of seismic demand and the variability in structural capacity caused by the sampled capacity curves within each building class.

For the estimation of the economic losses, each DS is associated with a loss ratio (i.e., 5% 20%, 60%, and 100% for slight, moderate, extensive and complete damage, respectively). For each building i , the expected loss is computed deterministically by identifying its DS ds_i from the peak roof displacement obtained in the NLTHA and then applying the following equation:

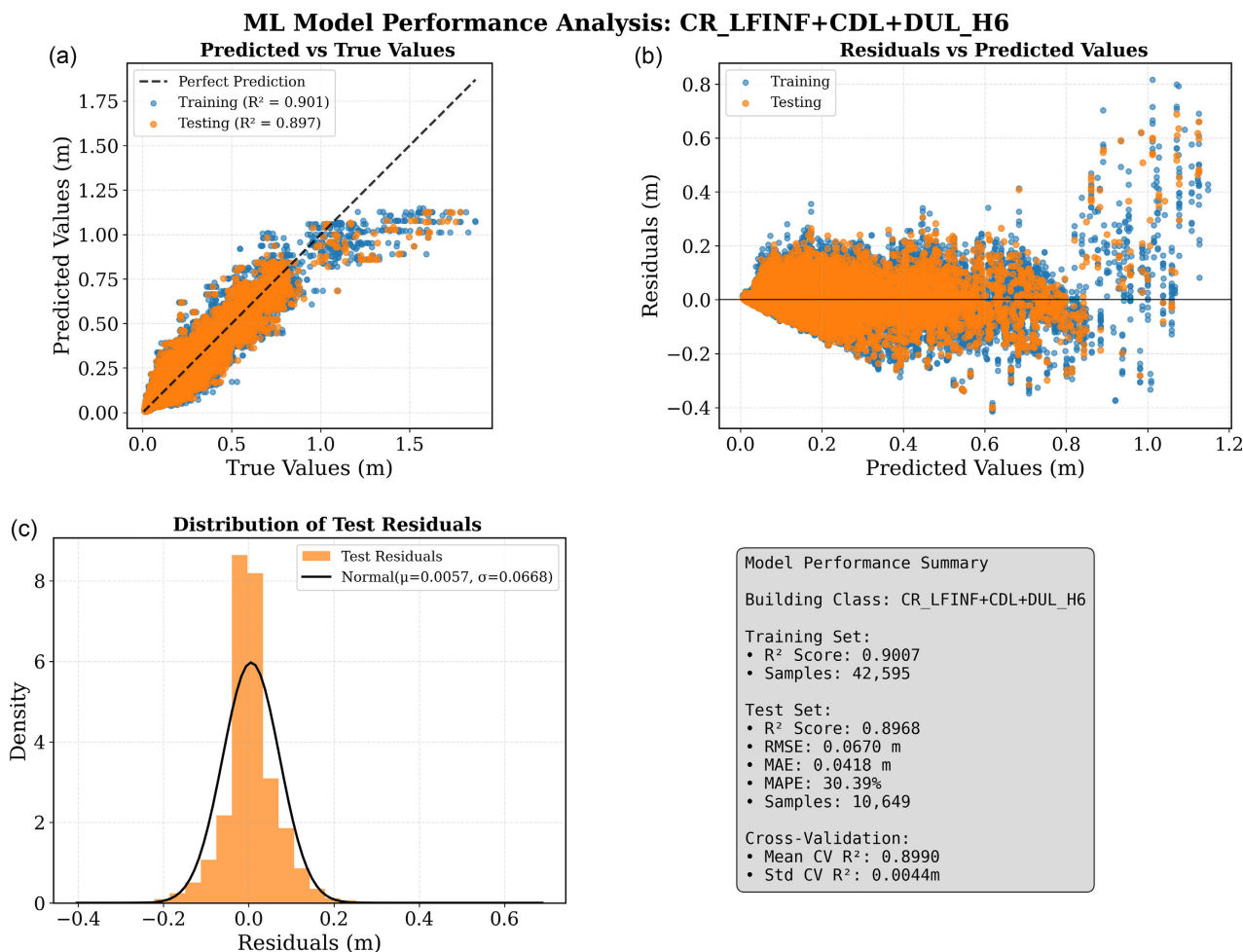


FIGURE 9 | ML model performance analysis for CR/LFINF + CDL + DUL/H6: (a) Predicted versus true values showing strong correlation ($R^2 = 0.907$ training, 0.917 testing), (b) residuals versus predicted values demonstrating model accuracy, and (c) distribution of test residuals with performance summary statistics including $RMSE = 0.042$ and cross-validation results.

$$L_i = V_i \times DLR(ds_i) \quad (1)$$

where V_i denotes the building’s replacement value, ds_i is the assigned DS, and $DLR(ds_i)$ is the damage loss ratio corresponding to that state. The total portfolio loss is simply the sum of the individual building losses: $L_{portfolio} = \sum_{i=1}^N L_i$. This process is repeated for all events within Subset 2. We assumed these losses to be the “true” direct economic impact for each event.

3.5 | Step 5 – Estimation of Losses Using the ML Model (Method B)

Portfolio losses for the Subset 2 events were computed using the ML model, assuming that only sensors on the ground exist, reflecting current rapid impact assessment practice in which recorded or estimated shaking is combined with fragility/vulnerability functions or ML models (e.g., Kalakonas and Silva 2022). For each event, the class-specific ML model was used to predict the expected maximum roof displacement for every building, which was then converted to an economic loss following the same procedure as Method A. It was assumed that seismic stations are installed within the study area, allowing IMs to be derived from records rather than ground motion models (GMMs). The implications of using GMMs with regard to the increase in bias and uncertainty are discussed later in this study.

3.6 | Step 6 – Estimation of Losses Using the Digital Twin (Method C)

This step introduces the theoretical framework underpinning the development of the proposed *digital twin*. For each building class c in our portfolio, a dedicated ANN model was developed, providing baseline ML predictions that form

Earthquake-Induced Building Damage State Distributions

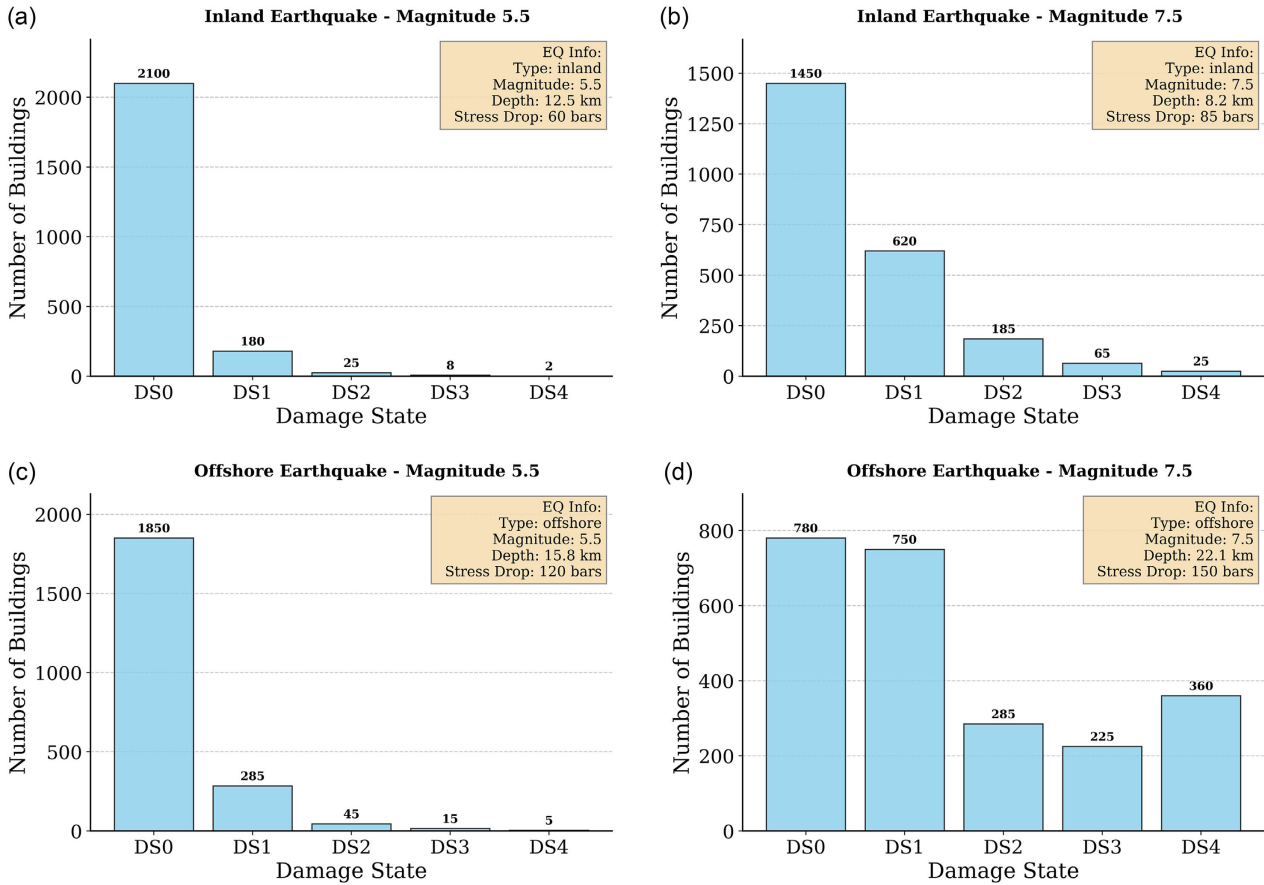


FIGURE 10 | Earthquake-induced building DS distributions: Comparison between (a,c) Inland earthquakes (Magnitude 5.5 and 7.5) and (b,d) offshore earthquakes (Magnitude 5.5 and 7.5), showing systematic differences in destructive potential with offshore events producing more severe damage distributions due to higher stress drops.

the foundation of the correlation-based conditioning framework. When an earthquake occurs and sensor measurements from instrumented buildings are available, prediction residuals are calculated as:

$$r_i = y_i^{obs} - \hat{y}_i^c \quad (2)$$

where y_i^{obs} is the observed response and \hat{y}_i^c is the ML-predicted response. These residuals encode information on systematic model bias and can be exploited to improve predictions for noninstrumented buildings through a building-to-building correlation model.

Operationalizing this approach requires the quantification of building-response uncertainties, the establishment of portfolio-wide correlation structures, and the development of a mathematical framework for propagating information from instrumented to noninstrumented buildings. To this end, a mixed-effects model was adopted to decompose the total uncertainty in building response as:

$$Y = \mu(IMs) + \varepsilon_E + \varepsilon_B \quad (3)$$

where Y is the natural logarithm of maximum roof displacement, $\mu(IMs)$ is the median prediction for a given set of IMs , ε_E is the between event variability with variance σ_E^2 , and ε_B is the building-to-building variability with variance σ_B^2 . Assuming that both sources of uncertainty are independent, the total variance in building response is expressed as:

$$\sigma^2 = \sigma_E^2 + \sigma_B^2 \quad (4)$$

The between event variability reflects aleatory uncertainty between different events (i.e., earthquakes with similar intensity can cause different structural responses due to differences in frequency content, duration, and other factors that affect

**Building Damage State Distribution - Rupture 950
Alvalade District, Lisbon**

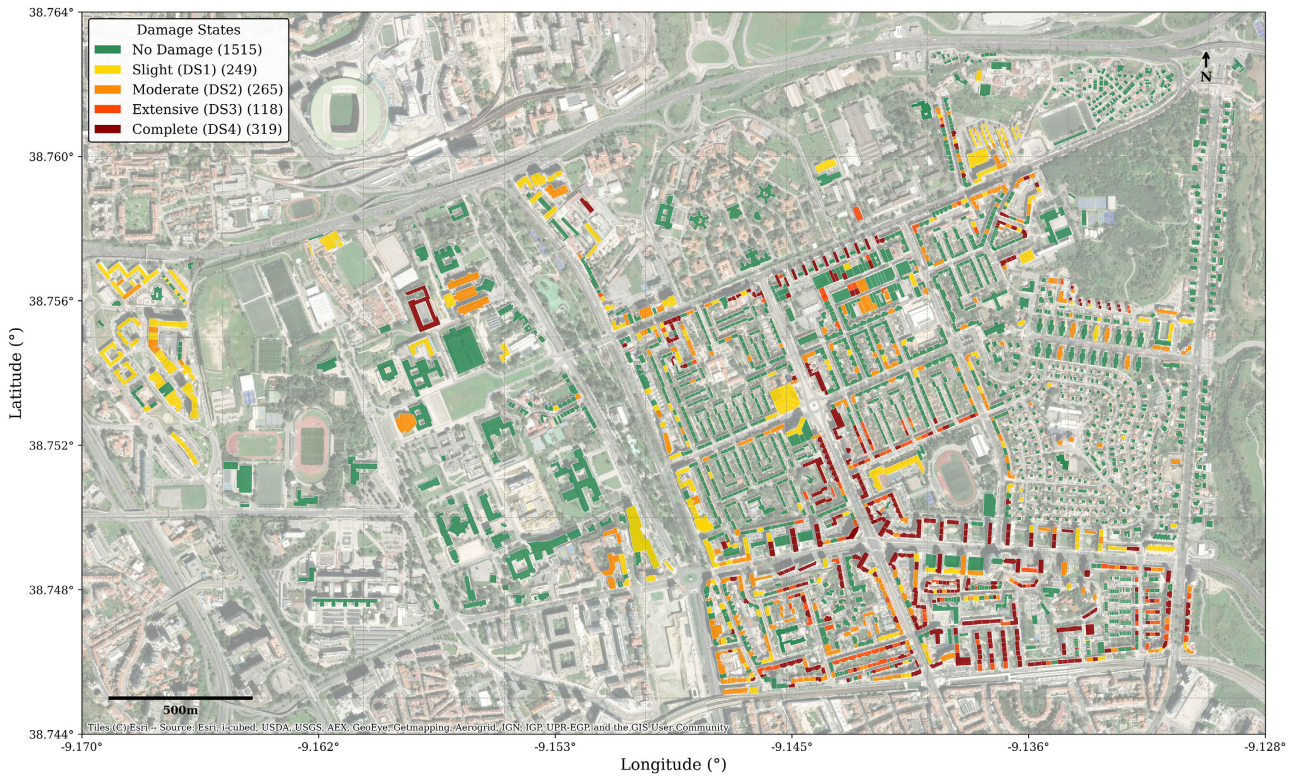


FIGURE 11 | Earthquake impact footprint - Alvalade parish, Lisbon: Building DS distribution showing spatial clustering of damage patterns with 1515 undamaged buildings, 265 moderate damage, 117 extensive damage, and 319 complete damage buildings.

all buildings within the same building class), while building-to-building variability arises from construction-related differences within a class (e.g., geometry, material properties).

A critical aspect of portfolio seismic risk analysis is recognizing that building responses are not independent but exhibit spatial and typological correlations (DeBock et al. 2014; Mejia and O'Reilly 2025). Buildings of the same building class tend to respond similarly to seismic excitation due to shared design principles, construction practices, and material properties. The correlation between the seismic responses of two buildings i and j is defined as:

$$\rho_{ij} = \frac{\text{Cov}(Y_i, Y_j)}{\sigma_i \times \sigma_j} \quad (5)$$

with typical values between 0.5 and 0.8 for buildings of the same class (DeBock et al. 2014; You and Tesfamariam 2024). The covariance structure is modeled as:

$$\Sigma = \sigma_B^2 \times R + \sigma_E^2 \times I \quad (6)$$

where R is the correlation matrix with off-diagonal elements ρ_{ij} for same-class buildings and zero otherwise, assuming there are no interclass response correlations, and I is the identity matrix. This formulation captures both the correlated component of response (through the building-to-building variability) and the independent component (through the record-to-record variability). Given the importance of this aspect for our study, mixed-effects analysis was applied to decompose the NLTHA-based response variability into σ_B and σ_E , and to estimate intraclass correlations.

The conditioning framework leverages the variance decomposition and correlation structure to update predictions for noninstrumented buildings based on sensor-informed residuals. This method explicitly separates the event-specific bias from building-specific deviations. This framework builds upon established methodologies in earthquake engineering for partitioning uncertainties in GMM, where different types of uncertainty components are properly separated and conditioned upon observational data (e.g., Engler et al. 2022; Silva et al. 2025). The event-specific bias, representing the systematic deviation of the actual ground motion effects from the predicted values, can be estimated as:

$$\varepsilon_E = \frac{E^T \Sigma_{B_1 B_1}^{-1} (y - \mu(IMS))}{1 + E^T \Sigma_{B_1 B_1}^{-1} E} \quad (7)$$

where E is a vector of ones, y is the vector of observed responses at instrumented buildings, $\mu(IMS)$ is the vector of prior predictions (which can be estimated using the ML models), and $\Sigma_{B_1 B_1}$ is the covariance matrix between instrumented buildings. This formulation represents a weighted average of the residuals at instrumented buildings, with weights determined by the inverse of the covariance matrix. The denominator acts as a shrinkage factor, preventing overconfidence when limited observations are available. The updated prediction for any noninstrumented building is then given by:

$$Y_{(conditioned)} = \mu(IMS) + \varepsilon_E E + \sigma_{B12B} \Sigma_{B11B}^{-1} w \quad (8)$$

where σ_{B12B} is the vector of covariances between instrumented buildings and any noninstrumented building of the same class, and w is the bias-corrected building residual calculated as:

$$w = y - \mu(IMS) - \varepsilon_E E \quad (9)$$

This approach effectively decomposes the observed residuals into a common event component (which affects all buildings) and building-specific components (which are correlated only among similar structures). The updating process naturally accounts for the reliability of observations through the covariance structure, giving more weight to observations from highly correlated buildings.

Unlike Methods A and B, the estimation of the economic losses using the *digital twin* is informed by the measurements of sensors, and thus the conditioned economic loss can be expressed by the following equation:

$$L_i^{conditioned} = V_i \times \text{DLR}(ds_i^{conditioned}) \quad (10)$$

The variable $L_i^{conditioned}$ represents the structural loss after applying conditioning corrections, demonstrating how response prediction improvements translate into more reliable loss estimates. Bias correction effectiveness can be quantified by comparing metrics before and after conditioning, with successful conditioning reducing both event-level and aggregate portfolio biases, as further explained in the following step.

3.7 | Step 7 – Evaluation of the Performance of the Digital Twin

The performance of the proposed *digital twin* was evaluated against both the benchmark results (Method A) and the state-of-practice approach (Method B). Since event-specific “true” losses have been derived directly from NLTHA simulations, the bias in portfolio economic loss for each seismic event p is computed as:

$$\text{Bias}_{event,p} = \frac{|L_{portfolio,p}^{predicted} - L_{portfolio,p}^{true}|}{L_{portfolio,p}^{true}} \times 100 \quad (11)$$

In addition to event-level comparisons, the overall accuracy of each method was evaluated through the computation of the total portfolio loss bias across all (N) events in the testing database. This aggregate metric captures systematic deviations in prediction performance and is defined as:

$$\text{Bias}_{total} = \frac{|\sum_{\{p=1\}}^N L_{portfolio,p}^{predicted} - \sum_{\{p=1\}}^N L_{portfolio,p}^{true}|}{\sum_{\{p=1\}}^N L_{portfolio,p}^{true}} \times 100 \quad (12)$$

These metrics provide a robust basis for evaluating how conditioning strategies improve loss prediction across a wide range of earthquake scenarios and intensity levels. In the subsequent analysis, variations in performance under different sensor deployment configurations across selected buildings are examined.

4 | Results

In this section, the results of the mixed-effects analysis and correlation model are presented, along with the performance of the *digital twin* under various sensor deployment configurations.

4.1 | Mixed-Effect Analysis and Correlation Estimation

The between-event and building-to-building variability in structural response residuals was quantified using a mixed-effects analysis (e.g., Stafford 2014), recognizing that prediction errors are not randomly distributed but exhibit correlation patterns reflecting both the physics of earthquake ground motion propagation and the spatial clustering of similar building types. In the mixed-effects approach, earthquake events are treated as random effects while systematic relationships between ground motion IMs and structural response are modeled, enabling the separation of variance components arising from event-to-event variability (σ_E) and building-to-building variability (σ_B) within the same seismic event. The analysis was implemented using the *statsmodels python* package (Seabold and Perktold 2010) with Powell optimization for numerical stability. Residuals from the ML predictions are used as the dependent variable, and earthquake rupture scenarios define the grouping structure. The model decomposes the total residual variance (σ_{total}) into its constituent components and calculates the intraevent correlation coefficient ($\rho = \sigma_E^2 / \sigma_{\text{total}}^2$), quantifying the degree to which buildings experience correlated response during the same earthquake.

Previous studies have examined spatial correlations in building seismic response parameters to improve regional loss assessment accuracy. DeBock et al. (2014) demonstrated significant spatial correlations in EDPs for closely spaced buildings (up to 25–65 km depending on earthquake magnitude), with stronger correlations observed between buildings having similar first-mode periods and structural characteristics. You and Tesfamariam (2024) investigated spatial correlations using a Gaussian random field approach but reported relatively weak cross-correlations between structurally dissimilar buildings, with correlations decaying rapidly with distance (approaching zero at ~ 10 km for some events). A key limitation acknowledged in both studies is the assumption that all buildings within the same structural class at different locations share identical capacity curves and structural properties. This simplification, while computationally necessary for regional assessments, may overestimate spatial correlations by assuming identical structural behavior among buildings of the same nominal class, potentially affecting the accuracy of regional loss estimates. Our study addresses this limitation by incorporating aleatory variability within each building class, as described in Step 1.

In addition to the mixed-effect analysis, pairwise correlation coefficients were calculated for each building class between all building pairs experiencing the same earthquake event, resulting in correlation matrices that capture how structural response varies across the portfolio under identical ground motion scenarios. This pairwise analysis highlights the correlated response patterns exhibited by buildings of similar construction types and spatial proximity.

The mixed-effects analysis results for the ten most prevalent building classes are summarized in Table 1, including the correlation parameters and variance decomposition components. Results presented in Figure 12 further indicate substantial variability in correlation patterns across building classes, with the overall distribution of correlation coefficients revealing a mean correlation of approximately 0.6 for the entire portfolio. The tabulated results show that the ML model performance (R^2 scores ranging from 0.84 to 0.90) aligns with residual correlation characteristics, as building classes with higher prediction accuracy tend to display more consistent correlation patterns. For the conditioning framework, a uniform correlation coefficient of $\rho = 0.6$ was applied across all building classes for simplicity and practical applicability, as in real world scenarios, the exact correlation structure for each class would not be known a priori without extensive calibration. Similarly, the variance decomposition revealed mean values of $\sigma^2_E = 0.6\sigma^2_{\text{total}}$ and $\sigma^2_B = 0.4\sigma^2_{\text{total}}$ across

TABLE 1 | Mixed-effects analysis results and correlation parameters by building class.

GEM taxonomy	N samples	R^2 score	RMSE	ρ	σ_E	σ_B	σ_{total}
MUR_LWAL + CDL_H2	694 260	0.835	0.017	0.53	0.012	0.011	0.017
MUR_LWAL + CDL_H4	570 024	0.905	0.023	0.60	0.017	0.016	0.023
CR_LFINF + CDL + DUL_H4	203 580	0.90	0.054	0.71	0.045	0.033	0.054
CR_LFINF + CDM + DUM_H2	199 404	0.841	0.028	0.62	0.022	0.020	0.028
CR_LFINF + CDL + DUL_H5	84 564	0.899	0.059	0.77	0.052	0.031	0.059
CR_LFINF + CDM + DUM_H4	58 464	0.909	0.042	0.61	0.033	0.028	0.042
CR_LFINF + CDL + DUL_H6	53 244	0.899	0.065	0.63	0.051	0.030	0.064
CR_LFINF + CDM + DUM_H10	49 068	0.897	0.080	0.73	0.068	0.047	0.080
CR_LFINF + CDL + DUL_H10	44 892	0.886	0.089	0.80	0.080	0.044	0.089
CR_LFINF + CDL + DUL_H2	41 760	0.876	0.033	0.52	0.024	0.025	0.033

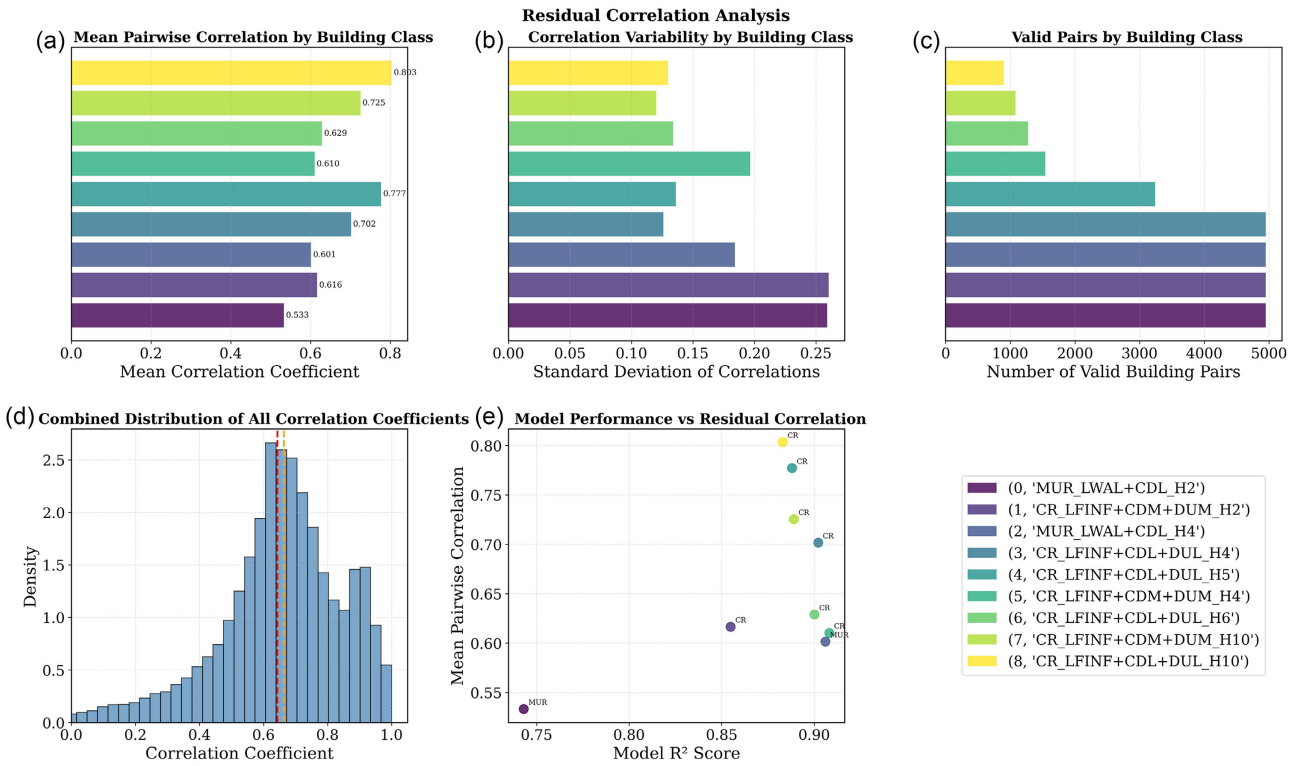


FIGURE 12 | Residual correlation analysis: (a) Mean pairwise correlation by building class, (b) correlation variability by building class, (c) valid pairs by building class, (d) combined distribution of all correlation coefficients showing mean correlation ~ 0.6 , and (e) model performance versus residual correlation relationships across building classes.

classes, which were applied uniformly in the conditioning algorithm. These representative parameters serve as prior distributions that guide the updating of damage predictions for unmonitored structures using sensor data.

These simulation-derived correlations are supported by empirical evidence of spatially correlated damage patterns observed in past earthquakes, where buildings of similar typology within localized areas experienced similar damage levels (e.g., 2009 M6.3 L'Aquila earthquake, [Del Gaudio et al. 2017](#)). That said, developing such correlation models empirically will become feasible once large-scale sensor networks are deployed and sufficient earthquake data are collected.

4.2 | Evaluation of the Performance of the Proposed Digital Twin

For the implementation of the proposed *digital twin*, sensors were assumed to be installed on the roofs of buildings belonging to the ten most common classes in the case study region, representing 85% of the total building stock in the Alvalade parish. Sensor configurations were designed to vary from 1 to 20 sensors per building class. For each configuration with n sensors per class, buildings were randomly sampled from their respective classes, and the conditioning analysis was repeated across multiple realizations to ensure results were representative rather than configuration specific. For a scenario with n sensors per class, the total number of instrumented buildings was $10n$, resulting in instrumentation densities ranging from 10 total sensors (minimal monitoring) to 200 total sensors (comprehensive monitoring) across the district.

The conditioning framework followed the theoretical approach described in Step 6 and utilized the uncertainty and correlation parameters presented in the previous subsection ($\sigma_{E^2} = 0.6\sigma_{total}^2$, $\sigma_{B^2} = 0.4\sigma_{total}^2$, $\rho = 0.6$) to construct spatial correlation matrices representing expected relationships between building responses during the same earthquake event. When observations from instrumented buildings became available, the conditioning equations were applied to propagate this information to noninstrumented buildings based on their expected correlation strengths, thereby correcting both systematic bias (epistemic uncertainty) and the random variability (aleatory uncertainty) in the original ML predictions.

Figure 13 presents the distributions of event-wise economic loss bias (Equation (11)) and the total bias across all events (Equation (12)). The results demonstrate substantial improvements in loss estimation when sensor observations were incorporated, with effectiveness increasing as more sensors were deployed. ML predictions exhibited a median

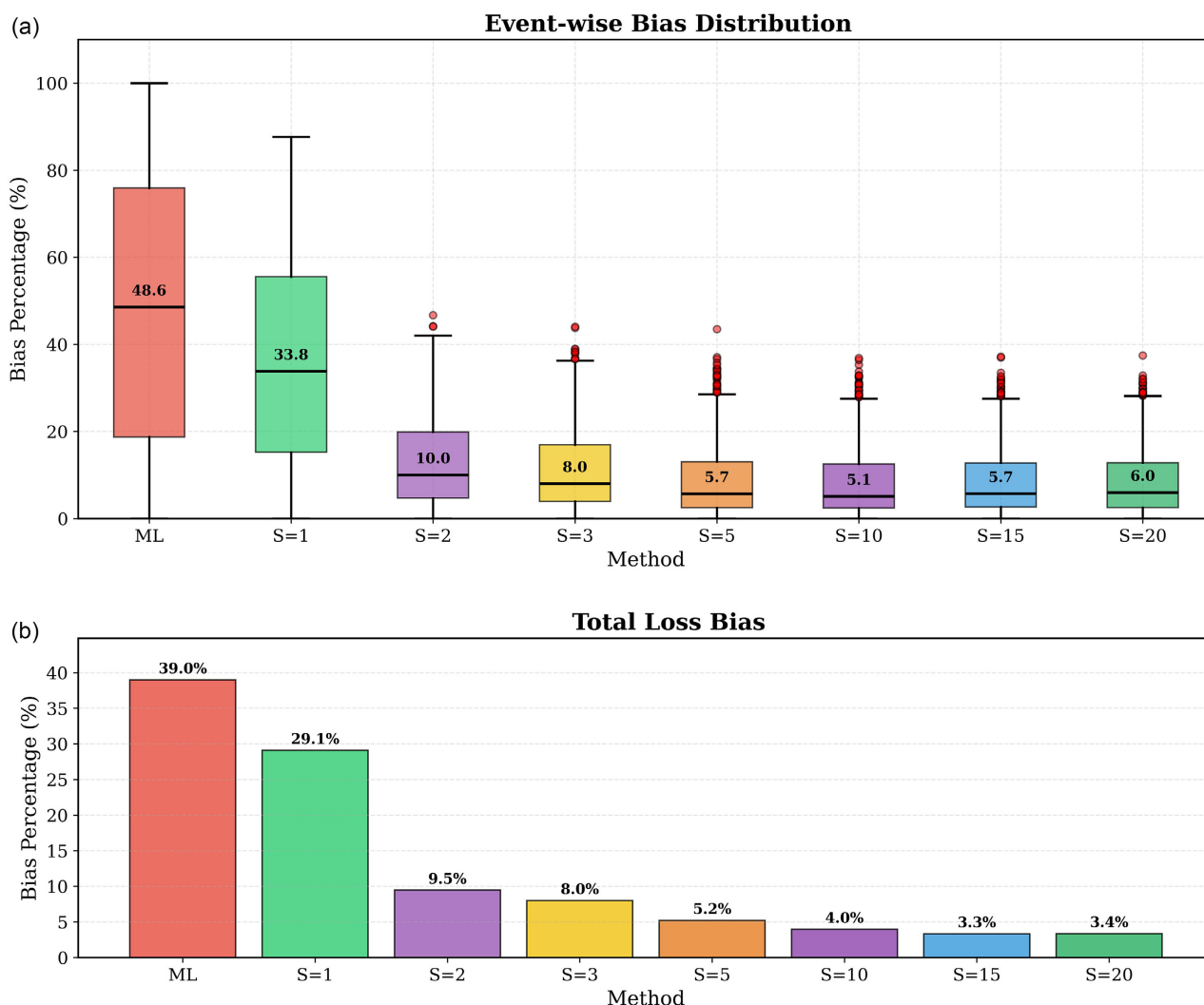


FIGURE 13 | Sensor deployment performance analysis: (a) Event-wise bias distribution showing systematic reduction from baseline ML (48.6%) through increasing sensor density per building class ($S = 1$ to $S = 20$), demonstrating optimal performance around $S = 3-5$ sensors per class. (b) Total loss bias comparison showing progressive improvement from 39.0% (ML baseline) to 3.4% ($S = 20$), with diminishing returns beyond moderate sensor deployment.

event-wise percentage bias of 48.6% relative to benchmark structural losses, reflecting the challenges of predicting non-linear structural responses. However, the use of sensor-informed conditioning substantially reduced these prediction errors, with systematic improvements observed as the number of instrumented buildings increased.

These results indicate that optimal instrumentation strategies benefit significantly from increased sensor network density, with the correlation-based approach producing consistent improvements in both event-wise and aggregate loss prediction metrics. Performance curves show that even moderate sensor deployments ($S = 2$) could yield significant gains, while comprehensive monitoring provides near-optimal accuracy for critical infrastructure applications, where precise damage assessment is essential for emergency response and recovery planning.

The correlation-based conditioning approach demonstrates systematic bias reduction that scales predictably with sensor density. With minimal instrumentation ($S = 1$, representing 1 sensor per class with 10 total sensors), the median event-wise percentage bias reduces significantly to 33.8%, representing a 30.3% improvement over the unconditioned baseline. This improvement becomes progressively more pronounced as sensor density increases, achieving median event-wise percentage biases of 10.0% with $S = 2$ (20 sensors), 8.0% with $S = 3$ (30 sensors), and continuing to improve through the higher sensor densities. The most comprehensive instrumentation scenario ($S = 20$, representing 20 sensors per class with 200 total sensors) achieves a median event-wise bias of only 6.0%, representing an 87.7% improvement compared to the unconditioned ML baseline. This systematic improvement illustrates how the physics-based correlation structure enables effective information propagation across the building network, with each additional sensor contributing

incrementally to overall prediction accuracy. The total loss prediction accuracy analysis provides complementary insights into the aggregate performance of the conditioning approach across the entire building portfolio.

Analysis of bias characteristics across a large sample of events reveals systematic patterns. The ML model overestimates losses in 66% of events, with mean bias strongly dependent on intensity: high bias at low PGA (69% for PGA 0.1-0.2 g) decreasing to near-optimal performance at high PGA (9% for PGA > 0.5 g). Similarly, bias is highest for low-loss events (82% for losses < 50) and lowest for severe events (4% for losses > 500). This intensity-dependent bias pattern explains why aggregate portfolio bias (39%) is lower than median event-wise bias (48.6%), which means large damaging events that dominate total losses exhibit lower prediction errors.

It is important to note that this study assumes sensor measurements are exact and free from measurement error, instrumentation noise, or placement uncertainties. This represents an idealized scenario that establishes an upper bound on the potential benefits of sensor integration. The quantified improvements in this study therefore represent a best-case scenario. Future work should investigate the robustness of the correlation-based conditioning framework to various levels of sensor noise and the trade-offs between sensor accuracy and deployment density.

Moreover, the current analysis assumes ground motion IMs are directly measured at the 20 seismic stations distributed across Alvalade. In practice, if GMMs were used instead of direct measurements, additional epistemic uncertainty would propagate through the conditioning framework. Studies have shown that GMM-based ground motion estimates can exhibit biases of 30%–50% (Silva et al. 2025), which would increase both the baseline ML prediction bias and reduce the effectiveness of sensor conditioning. This represents an important limitation that future operational systems must address through denser station networks or improved ground motion interpolation methods.

5 | Conclusions

A numerical framework for the testing and design of a digital twin for rapid earthquake impact assessment was proposed in this study, using a building portfolio of 2457 structures in the Alvalade civil parish of Lisbon (Portugal) as a case study. This virtual experiment uses synthetic earthquake scenarios and simulated building responses to validate the methodology and establish performance benchmarks for future operational deployment. The *digital twin* comprises an idealized numerical representation of each building using MDOF stick-and-mass models, a ML model that predicts roof displacement for each building class, and a network of sensors both at the ground (to capture spatial variations in ground shaking) and on the roofs of selected buildings from the ten most common building classes.

It was observed that even a minimal sensor deployment can substantially improve the estimation of economic losses. With just 20 sensors (two per building class), correlation-based conditioning reduced prediction bias by 38.6%. This improvement arises from the spatial correlation of building responses to earthquakes, whereby data from one representative building provides insights into others of the same type. The results demonstrate that seismic patterns enable the generalization of structural behavior across similar buildings.

The correlation-based conditioning approach was found to excel in overall loss estimation and to scale effectively with increasing sensor density, as it adjusts for both event- and building-specific biases. These findings highlight that moderate, strategically placed sensor networks are more cost-effective than widespread deployments, offering significant benefits for emergency responses where rapid loss estimates are critical. Compared to conventional loss estimation tools, which often exhibit biases exceeding 50% and lack real-time adaptation, the proposed digital twin framework provides substantially improved prediction accuracy by integrating real-time observations with physics-informed models.

While promising, this study was based on simulations, meaning real-world uncertainties related to seismic wave propagation or sensor anomalies are not fully captured. Additionally, the use of a single correlation coefficient for all buildings may oversimplify the true complexity of seismic response patterns. Furthermore, the limited spatial extent of the study area (building distances ≤ 5 km) restricts correlation estimates primarily to event-related response coherence, excluding distance-dependent correlation reductions observed in larger regional analyses, potentially leading to overestimated correlations unsuitable for broader applications. Furthermore, it was assumed that ground shaking was accurately measured at the 20 sensor locations; had GMMs been used instead, prediction bias and uncertainty would likely have been higher (Silva et al. 2025). Future work should validate these findings through real-world sensor deployments in seismic regions. More advanced correlation models are needed to account for variations in earthquake behavior and building proximity. Expanding analyses to larger geographic regions is essential to incorporate spatial decay effects and to develop distance-dependent correlation models, enabling more generalizable results for regional seismic loss assessments.

Acknowledgments

The first author acknowledges the support of the Portuguese Foundation for Science and Technology (FCT) through PhD scholarship 2022.12609.BD. The authors are grateful to the two anonymous reviewers and the Associate Editor for their constructive comments and suggestions, which significantly improved the quality of this manuscript.

Conflicts of Interest

The authors declare no conflicts of interest.

Data Availability Statement

The machine learning models developed and used in this study are publicly available at the following GitHub repository: <https://github.com/amirt1994/Alvalade-seismic-digital-twin>.

Endnotes

¹ <https://github.com/GEMScienceTools/oq-vmrk>.

References

- Bolton, A., L. Butler, I. Dabson, et al. 2018. *The Gemini Principles*. University of Cambridge. <https://doi.org/10.17863/CAM.32260>.
- Boore, D. 2003. "Simulation of Ground Motion Using the Stochastic Method." *Pure and Applied Geophysics* 160: 635–676. <https://doi.org/10.1007/PL00012553>.
- Brucherseifer, E., H. Winter, A. Mentges, M. Mühlhäuser, and M. Hellmann. 2025. "A Data Taxonomy Towards the Applicability of the Digital Twin Conceptual Framework in Disaster Management." *ArXiv* <https://doi.org/10.48550/arXiv.2503.00076>.
- Dal Zilio, L., D. Giardini, R. Carbonell, and S. Wiemer. 2023. "Harnessing the Potential of Digital Twins in Seismology." *Nature Reviews Earth & Environment* 4: 510–512. <https://doi.org/10.1038/s43017-023-00469-y>.
- Danciu, L., S. Nandan, C. Reyes, et al. 2021. "The 2020 Update of the European Seismic Hazard Model: Model Overview." *EFEHR Technical Report 001 v1.0.0*. <https://doi.org/10.12686/a15Report>.
- DeBock, D. J., J. W. Garrison, K. Y. Kim, and A. B. Liel. 2014. "Incorporation of Spatial Correlations between Building Response Parameters in Regional Seismic Loss Assessment." *Bulletin of the Seismological Society of America* 104, no. 1: 214–228. <https://doi.org/10.1785/0120130137>.
- Del Gaudio, C., G. De Martino, M. Di Ludovico, et al. 2017. "Empirical Fragility Curves from Damage Data on RC Buildings after the 2009 L'Aquila Earthquake." *Bulletin of Earthquake Engineering* 15: 1425–1450. <https://doi.org/10.1007/s10518-016-0026-1>.
- Dogan, G., J. Tang, T. Arslan, J. Ploennigs, and H. Hagrass. 2021. "Digital Twin Based Disaster Management System Proposal: DT-DMS." *ArXiv*, <https://doi.org/10.48550/arXiv.2103.17245>.
- Engler, D. T., C. B. Worden, E. M. Thompson, and K. S. Jaiswal. 2022. "Partitioning Ground Motion Uncertainty When Conditioned on Station Data." *Bulletin of the Seismological Society of America* 112, no. 2: 1060–1079. <https://doi.org/10.1785/0120210177>.
- Erdik, M. 2017. "Earthquake Risk Assessment." *Bulletin of Earthquake Engineering* 15: 5055–5092. <https://doi.org/10.1007/s10518-017-0235-2>.
- Farrar, C. R., and K. Worden. 2012. *Structural Health Monitoring: A Machine Learning Perspective*. John Wiley & Sons. <https://doi.org/10.1002/9781118443118>.
- Federal Emergency Management Agency. 2020. "Hazus-MH 2.1 Technical Manual: Earthquake Model." US Department of Homeland Security. https://www.fema.gov/sites/default/files/2020-09/fema_hazus_earthquake-model_technical-manual_2.1.pdf.
- Ford, D. N., and C. M. Wolf. 2020. "Smart Cities with Digital Twin Systems for Disaster Management." *Journal of Management in Engineering* 36, no. 4: 04020027.
- Giordano, N., R. De Risi, J. Macdonald, et al. 2023. "Implications of Building Code Enforcement and Urban Expansion on Future Earthquake Loss in East Africa: Case Study—Blantyre, Malawi." *Natural Hazards* 117: 1083–1104. <https://doi.org/10.1007/s11069-023-05895-1>.
- Grieves, M. 2002. *Conceptual Ideal for PLM. Product Lifecycle Management Executive Summary*. University of Michigan.
- Habib, Z., H. Alshahrani, S. Saeed, and S. Nazir. 2025. "Exploring the Sustainability Benefits of Digital Twin Technology in Achieving Resilient Smart Cities During Strong Earthquake Events." *Arabian Journal for Science and Engineering* 50: 16869–16883. <https://doi.org/10.1007/s13369-025-10017-z>.

- He, C., Q. Huang, X. Bai, et al. 2021. "A Global Analysis of the Relationship Between Urbanization and Fatalities in Earthquake-Prone Areas." *International Journal of Disaster Risk Science* 12: 805–820. <https://doi.org/10.1007/s13753-021-00385-z>.
- Hoskere, V., Y. Narazaki, T. A. Hoang, and B. F. Spencer. 2022. "Vision-Based Structural Inspection Using Multiscale Deep Convolutional Neural Networks." *Sensors* 22, no. 11: 4178.
- Kalakonas, P., and V. Silva. 2022. "Seismic Vulnerability Modelling of Building Portfolios Using Artificial Neural Networks." *Earthquake Engineering & Structural Dynamics* 51: 310–327. <https://doi.org/10.1002/eqe.3567>.
- Khaloo, A. R., and H. Khosravi. 2013. "Modified Fish-Bone Model: A Simplified MDOF Model for Simulation of Seismic Responses of Moment Resisting Frames." *Soil Dynamics and Earthquake Engineering* 55: 195–210.
- Kusakabe, T., H. Yamazoe, A. Furukawa, and S. Kanai. 2021. "Development of Urban High-Fidelity CFD Model for Multi-Physical Earthquake Simulation." *Journal of Physics: Conference Series* 1736, no. 1: 012015.
- Levine, N. M., and B. F. Spencer. 2022. "Post-Earthquake Building Evaluation Using UAVs: A BIM-Based Digital Twin Framework." *Sensors* 22, no. 3: 873.
- Li, C. 2022. "Research on Urban Flood Disaster Assessment Based on Digital Twin." *Remote Sensing* 14, no. 15: 3533.
- Li, S., and F. Brennan. 2024. "Digital Twin Enabled Structural Integrity Management: Critical Review and Framework Development." *Proceedings of the Institution of Mechanical Engineers, Part M: Journal of Engineering for the Maritime Environment* 238, no. 4: 707–727. <https://doi.org/10.1177/14750902241227254>.
- Lin, Y., J. Kang, and C. C. Chang. 2021. "Seismic Collapse Probability Evaluation of Steel Moment Frames Using Artificial Neural Networks." *Earthquake Engineering and Structural Dynamics* 50, no. 6: 1433–1452.
- Lu, Q., A. K. Parlikad, P. Woodall, et al. 2020. "Developing a Digital Twin at Building and City Levels: Case Study of West Cambridge Campus." *Journal of Management in Engineering* 36, no. 3: 05020004.
- Martins, L., and V. Silva. 2021. "Development of a Fragility and Vulnerability Model for Global Seismic Risk Analyses." *Bulletin of Earthquake Engineering* 19: 6719–6745. <https://doi.org/10.1007/s10518-020-00885-1>.
- Mejia, T., and G. J. O'Reilly. "Quantifying the Impacts of Incorporating Damage Correlation on Scenario-Based Regional Seismic Assessment." *Earthquake Engineering & Structural Dynamics* 55 (2025): 94–111. <https://doi.org/10.1002/eqe.70069>.
- Mikell, A., and T. Mikell. 2018. "Digital Twin: From Concept to Reality." SAE Technical Paper, 2018-01-1381.
- Mohammadi, N., and J. E. Taylor. 2017. "Smart City Digital Twins." in IEEE Symposium Series on Computational Intelligence (SSCI). 1–5.
- Mohammadi, N., and J. E. Taylor. 2021. "Thinking Fast and Slow in Disaster Decision-Making with Smart City Digital Twins." *Nature Computational Science* 1: 771–773. <https://doi.org/10.1038/s43588-021-00174-0>.
- Nafeh, A. M. B., K. Aljawhari, and V. Silva. 2025. "An Open-Source Toolkit for Seismic Vulnerability Assessment." In Proceedings of the 10th ECCOMAS Thematic Conference on Computational Methods in Structural Dynamics and Earthquake Engineering (COMPdyn25).
- Ozsarac, V., N. Pereira, H. Mohamed, X. Romão, and G. J. O'Reilly. 2025. "The Built Environment Data Framework for Simulated Design and Vulnerability Modelling in Earthquake Engineering." *Earthquake Engineering & Structural Dynamics* 54: 2651–2670. <https://doi.org/10.1002/eqe.4378>.
- Pantoja-Rosero, B. G., R. Achanta, M. Kozinski, P. Fua, F. Perez-Cruz, and K. Beyer. 2023. "Image-Based Geometric Digital Twinning for Stone Masonry Elements." *Automation in Construction* 145: 104632.
- Pregolato, M., A. Ford, S. M. Wilkinson, and R. J. Dawson. 2022. "The Impact of Flooding on Road Transport: A Depth-Disruption Function." *Transportation Research Part D: Transport and Environment* 55: 67–81.
- Seabold, S. and J. Perktold. 2010. "Statsmodels: Econometric and Modeling with Python." 9th Python in Science Conference, Austin, 28 June–3 July, 2010, 57–61.
- Silva, V., D. Wald, and A. Taherian. 2025. "Potential Benefits of Seismic Monitoring for Ground-Shaking Estimation and Loss Assessment." *Bulletin of the Seismological Society of America* 115: 1658–1676. <https://doi.org/10.1785/0120240014>.
- Silva, V., H. Crowley, H. Varum, R. Pinho, and R. Sousa. 2014. "Evaluation of Analytical Methodologies Used to Derive Vulnerability Functions." *Earthquake Engineering and Structural Dynamics* 43: 181–204.
- Silva, V., R. Sousa, F. Ribeiro Gouveia, J. Lopes, and M. J. Guerreiro. 2024. "A Building Imagery Database for the Calibration of ML Algorithms." *Earthquake Spectra* 40, no. 2: 1577–1590. <https://doi.org/10.1177/87552930241229103>.
- Silva, V., S. Brzez, C. Scawthorn, C. Yepes, J. Dabbeek, and H. Crowley. 2022. "A Building Classification System for Multi-Hazard Risk Assessment." *International Journal of Disaster Risk Science* 13: 161–177. <https://doi.org/10.1007/s13753-022-00400-x>.
- Stafford, P. J. 2014. "Crossed and Nested Mixed-Effects Approaches for Enhanced Model Development and Removal of the Ergodic Assumption in Empirical Ground-Motion Models." *Bulletin of the Seismological Society of America* 104, no. 2: 702–719. <https://doi.org/10.1785/0120130145>.

- Stewart, J. P., G. A. Parker, G. M. Atkinson, D. M. Boore, Y. M. A. Hashash, and W. J. Silva. 2020. "Ergodic Site Amplification Model for Central and Eastern North America." *Earthquake Spectra* 36, no. 1: 42–68. <https://doi.org/10.1177/8755293019878185>.
- Taherian, A., V. Silva, P. Kalakonas, and R. Vicente. 2024. "An Earthquake Ground-Motion Model for Southwest Iberia." *Bulletin of the Seismological Society of America* 114, no. 5: 2613–2638. <https://doi.org/10.1785/0120230250>.
- Xie, W., Z. Yang, S. Li, and H. Chen. 2025. "AIoT-Powered Building Digital Twin for Smart Firefighting and Super Real-Time Fire Forecast." *Advanced Engineering Informatics* 53: 102745.
- Ye, C., L. Butler, B. Calka, et al. 2019. "A Digital Twin of Bridges for Structural Health Monitoring." <https://doi.org/10.12783/shm2019/32287>.
- You, T., and S. Tesfamariam. 2024. "Spatial Correlation in Building Seismic Performance for Regional Resilience Assessment." *Resilient Cities and Structures* 3: 57–65. <https://doi.org/10.1016/j.rcns.2024.06.004>.
- Yu, S., Q. Lei, C. Liu, N. Zhang, S. Shan, and X. Zeng. 2023. "Application Research on Digital Twins of Urban Earthquake Disasters." *Geomatics, Natural Hazards and Risk* 14, no. 1. <https://doi.org/10.1080/19475705.2023.2278274>.
- Zhao, D., Z. Wang, J. Wang, et al. 2023. "A Rapid Estimation Method for Post-Earthquake Building Losses." *International Journal of Disaster Risk Science* 14: 428–439. <https://doi.org/10.1007/s13753-023-00491-0>.